Morphological Behavior of Compositionally Gradient Polystyrene-Polylactide Bottlebrush Copolymers

*Liuyin Jiang,† Dmytro Nykypanchuk,‡ Vincent J. Pastore,† and Javid Rzayev†**

†Department of Chemistry, University at Buffalo, The State University of New York, Buffalo, New York 14260-3000, United States

‡ Center for Functional Nanomaterials, Brookhaven National Laboratory, Upton, New York 11973, United States.

Keywords: bottlebrush copolymers, self-assembly, gradient polymers, morphology, small angle x-ray scattering, nanostructure

ABSTRACT

Morphological behavior of PS-PLA bottlebrush copolymers with a compositional gradient along the backbone was investigated by small-angle X-ray scattering (SAXS) analysis and compared to that of their block copolymer analogs. Side-chain-symmetric gradient copolymers with varying volume fractions were prepared by one-step ring-opening metathesis polymerization of the corresponding *exo*- and *endo*-norbornene-functionalized macromonomers of similar lengths. The morphological map constructed using the SAXS data revealed a wide cylindrical morphology window, including for symmetric compositions, well-ordered lamella morphologies at very low PS volume fractions, and the formation of a rare bicontinuous gyroid morphology. In addition to the highly asymmetric nature of the morphology diagram, the domain spacings obtained for gradient bottlebrush copolymers were significantly smaller (by 30-40%) than the corresponding bottlebrush block copolymer analogs, which was attributed to a non-perpendicular orientation of the gradient bottlebrush backbone at the domain interface. Side-chain-asymmetric gradient bottlebrush copolymers were synthesized from PS and PLA macromonomers of different lengths and were demonstrated to assemble into well-ordered cylindrical and lamella morphologies. The results of these studies demonstrate that the gradient interface plays an important role in determining molecular packing during bottlebrush copolymer self-assembly. A rich morphological behavior of the gradient bottlebrush copolymers combined with their "user-friendly" one-step synthesis provides a robust and versatile platform for nanostructured materials design and fabrication.

Introduction

Melt state self-assembly of block copolymers has been extensively used for fabricating materials with nanoscale morphologies, which are being developed for applications as membranes, templates for nanomaterial fabrication, surface patterning, and catalyst supports.[1-6] Self-assembly behavior of an AB diblock copolymer is governed by the segregation strength parameter, $\chi_{AB}N$ and polymer composition parameter f_A, where χ_{AB} is the Flory-Huggins interaction parameter between A and B segments, N is the overall degree of polymerization, and f_A is the volume fraction of block A.[7-8] Linear diblock copolymers with carefully controlled block lengths can produce a wide variety of morphologies including lamellar, cylindrical, gyroid and spherical.[9-10] Recently, bottlebrush copolymers (BCP) have emerged as a new class of macromolecules featuring densely grafted side chains, molecular rigidity, low density of entanglements and fast assembly kinetics in the melt state.[11-14] These unique characteristics have allowed bottlebrush block copolymers to be used in the preparation of materials that are difficult to access with linear systems, e.g. photonic nanostructures with very large domain spacings (>150 nm).[15-18] Due to their rigidity, block BCPs show a strong propensity for lamellar morphologies. In this paper, we demonstrate a vastly different and richer phase behavior of bottlebrush copolymers featuring a gradient compositional profile along the backbone.

Block BCP composition can be manipulated by backbone or side chain asymmetry. The strong tendency of side-chain-symmetric bottlebrush block copolymers to pack into lamellar microstructures has been well documented.[19-21] Such bottlebrush block copolymers require a high degree of backbone asymmetry to form non-lamella morphologies. For example, Gai et al. found that polystyrene-poly(ethylene oxide) (PS-PEO) bottlebrush block copolymers form cylindrical

morphologies only at high degrees of asymmetry ($f_{PEO} \sim 0.8$).[20] Bates et al. reported the formation of a cylindrical morphology from PS-PEO-PS triblock bottlebrush copolymer with $f_{PEO} > 0.75$.[22] For side-chain-symmetric polystyrene-polylactide (PS-PLA) bottlebrush block copolymers with a vinyl backbone, lamellar morphology was observed even for asymmetric compositions, while cylindrical morphology was obtained only when significant side chain asymmetry was introduced.[19] Non-lamellar morphologies were also observed from other bottlebrush copolymers with extreme side chain asymmetries, such as brush-linear block copolymers.[18, 23-24] A greater morphological diversity has been observed in statistical or Janus-type bottlebrush copolymers, including cylindrical and gyroid phases.[25-26] Phase separation of such BCPs, which are comprised of linear diblock copolymers tethered together through the junction points, is driven by their side chains, and therefore, their morphological behavior, including the length scale of the obtained nanostructures, parallels that of the constituent linear block copolymers. These examples illustrate the effect of molecular structure on polymer assembly, and set the stage for exploiting bottlebrush architecture as a powerful handle for morphological control.

There has been an increased research focus on incorporating gradient structural changes in bottlebrush polymers. For example, Grubbs et al.[27] and Matyjaszewski et al.[28-29] reported the synthesis of bottlebrush polymers with gradient grafting densities using 'grafting-through' and 'grafting-from' strategies, respectively. Tapered bottlebrush polymers with gradually changing side-chain lengths have been synthesized by Matson et al. by sequential ring-opening metathesis polymerization (ROMP) of macromonomers with varying lengths.[30] Bottlebrush copolymers with changing cross-sectional diameters were also prepared using continuous flow chemistry by Guironnet et al.[31] Choi et al. reported the synthesis of gradient polymers with dendritic side chains through the use of dendronized macromonomers functionalized with cyclic olefins

exhibiting different reactivities.[32] Recently, we reported the synthesis of bottlebrush copolymers with a gradient compositional profile along the backbone by a one-step ROMP of two macromonomers with vastly different reactivities that contained *exo*- and *endo*-norbornene end groups (Figure 1).[33] We demonstrated that side-chain-symmetric and compositionally symmetric gradient bottlebrush copolymers pack into cylindrical microstructures, in contrast to their block and statistical bottlebrush analogs. In this paper, we undertake a detailed evaluation of the morphological behavior of compositionally gradient bottlebrush copolymers by small angle X-ray scattering (SAXS). We construct a morphological map for side-chain-symmetric gradient bottlebrushes with varying backbone asymmetries, which includes the formation of cylindrical morphology over a wide compositional window and the presence of a rare bottlebrush gyroid morphology. We also present results on the synthesis and self-assembly of compositionally gradient and side-chain-asymmetric, or "cone-shaped" bottlebrush copolymers. Our results demonstrate that the gradient interface has a dramatic impact on the assembly of bottlebrush copolymers, which can be harnessed for enriching their morphological behavior.

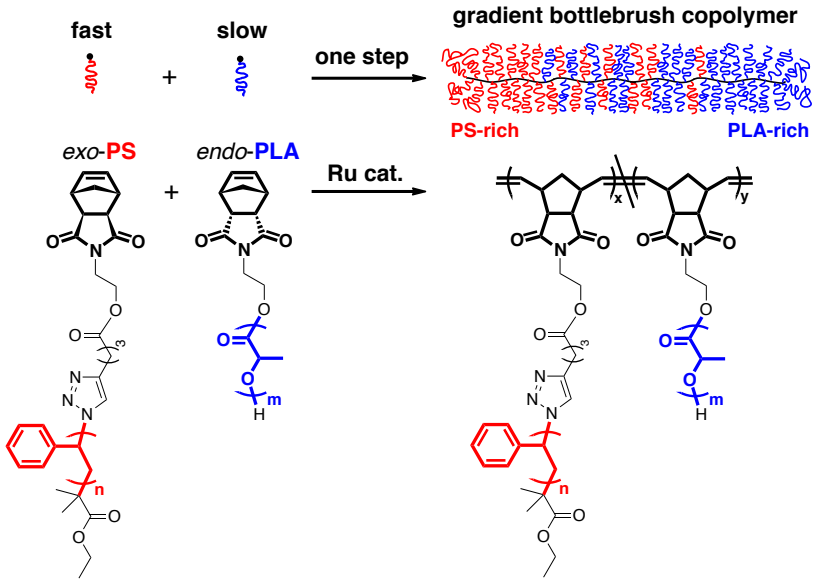

Figure 1. One-step synthesis of gradient bottlebrush copolymers by ring-opening metathesis polymerization using *exo*-norbornene-functionalized PS and *endo*-norbornene-functionalized PLA macromonomers.

Experimental Section

Materials and Measurements. Solvents and reagents were purchased from commercial sources and used directly without purification unless noted. *Exo*- and *endo*-norbornene-functionalized macromonomers *exo*-PS (2.2 kg/mol), *exo*-PLA (2.0 kg/mol), *endo*-PLA (2.1 kg/mol) and *endo*-PLA (3.7 kg/mol) (Figures S1-S4, Supporting Information) were synthesized using previously reported procedures.[34] ^{1}H NMR spectra were recorded with Inova-500 MHz spectrometers and chemical shifts were reported in ppm using TMS or deuterated solvents as internal standards ($CDCl_3$, 7.27 ppm). Size exclusion chromatography analysis was performed by using Viscotek's GPC Max system with and two PLgel PolyPore columns (Agilent), and TDA 302 Tetra detector

Array system equipped with refractive index, UV, viscosity, low (7°), and right angle light scattering units. Tetrahydrofuran was used as a mobile phase at 30 °C. The system was calibrated with 10 polystyrene standards from 1.2×10^6 to 500 g/mol. For gradient BCP samples, molecular weights were determined by SEC-LS using d*n*/d*c* calculated based on weight fractions of PS (d*n*/d*c* = 0.185 mL/g) and PLA (d*n*/d*c* = 0.042 mL/g). For block BCP samples, molecular weights of the first block were determined by SEC-LS, while the length of the second block was determined by ^{1}H NMR analysis based on the integral ratios of signals coming from the aromatic PS protons (2*H*, 6.3-6.9 ppm) and methine protons of the PLA repeat unit (1*H*, 5.2 ppm). Scanning Electron Microscopy (SEM) images were obtained on a Carl Zeiss AURIGA instrument with a 2 keV accelerating voltage and a secondary electron detector. Freshly fractured monolith of copolymer **G6** was soaked in 0.5 M NaOH aqueous methanol solution (50/50 by volume) for 20 minutes at 50 °C to improve topographic contrast, and was gold-coated for 60 s using an SPI-Module sputter coater prior to imaging. SAXS data were collected either on a custom SaxsLab instrument or at the 11-BM (CMS) beamline of the National Synchrotron Light Source II (NSLS-II) of Brookhaven National Laboratory. The SaxsLab instrument was equipped with a PILATUS 300K area detector and a rotating copper anode. The CMS beamline was equipped with PILATUS 2M area detector and x-ray energy was set to 13.5keV. The sample to detector distance was calibrated with silver behenate for both SaxsLab instrument and CMS beamline. Image reduction and conversion to intensity vs scattering vector *q* was performed with Saxsgui package (saxsgui.com). Temperature-dependent SAXS experiments were done on SaxsLab instrument using a Linkham Scientific temperature stage. The polymer sample was sandwiched between Kapton windows and placed in a metal holder. Care was taken to ensure good contact between the sample, the holder and the temperature stage. The polymer sample was

brought to a desired temperature using heating and cooling rates of 0.5 °C per min, and equilibrated for 30 min before starting the measurements with a typical exposure time of 1 h.

PS and PLA bottlebrush persistence length determination. For persistence length (l_p) measurements, filtered polymer solutions were placed in 1 mm diameter glass capillary tubes (Charles Supper, MA). For background subtraction, we also measured scattering from the corresponding solvents under analogous conditions. Different concentrations of polymer solutions were tested from 1 to 10 mg/ml. We found 2 mg/ml to be optimal, providing a good signal to noise ratio without a discernible effect of chain overlap on the scattering. The data analysis was done with SasView 4.1.2 software package.[35] To determine persistence length, we have used flexible cylinder model, which is a good approximation for semirigid macromolecules.[36] The polydispersity of backbone and side chains were accounted for using Schulz distribution function.

General procedure for PS_n-*grad*-PLA_m BCP synthesis. In a 1-dram vial, a mixture of *exo*-PS and *endo*-PLA macromonomers with a predetermined feed ratio was dissolved in a degassed anhydrous dichloromethane at $[M]_0 = 0.05M$ in the glove box under argon. In a separate vial, a stock solution of 3rd generation Grubbs' catalyst was prepared. An aliquot was withdrawn from the macromonomer mixture before the addition of a desired amount of catalyst stock solution. Reaction was allowed to run overnight and quenched with ethyl vinyl ether. A small sample was withdrawn for GPC analysis. The rest of the reaction mixture was precipitated into methanol and dried in vacuo.

General procedure for PS_n-*block*-PLA_m BCP synthesis. In a glove box, *exo*-PLA was dissolved in dry DCM (0.2 g/ml) in a 1-dram vial equipped with a stir bar. *Exo*-PS was dissolved with dry

DCM (0.1 g/ml) in a separate vial. A catalyst stock solution (1 mg/mL) was made by dissolving 3rd generation Grubbs' catalyst in dry DCM. Polymerization was initiated by adding desired catalyst stock solution to the *exo*-PLA solution. The reaction was allowed to run for 45 min before an aliquot was withdrawn. The aliquot was immediately quenched by ethyl vinyl ether and analyzed by SEC without further purification. *Exo*-PS solution was then added to the reaction. The polymerization was allowed to run for another 60 min before quenching with ethyl vinyl ether. A small aliquot was extracted for SEC and NMR analysis and the rest was precipitated into methanol.

Results and Discussion

Polymer synthesis

Exo-norbornene-capped PS macromonomer (*exo*-PS 2.2 kg/mol) was prepared by conjugating azide-terminated polystyrene and *exo*-norbornene functionalized alkyne using copper mediated azide-alkyne click chemistry.[34] *Exo*- and *endo*-norbornene-capped PLA macromonomers (*exo*-PLA 2.0 kg/mol, and *endo*-PLA 2.1 kg/mol) were synthesized by ring-opening polymerization of D,L-lactide from the corresponding norbornene-functionalized initiator. PS(2.2k)$_n$-*grad*-PLA(2.1k)$_m$ bottlebrush copolymers were prepared by one-step copolymerization of *exo*-PS and *endo*-PLA macromonomers using the 3rd generation Grubbs' catalyst (Figure 2 top). We have previously reported a kinetic study of this copolymerization, which verified the formation of compositionally gradient copolymers composed of PS-rich and PLA-rich end segments (blocks) and a gradient interface between the two blocks.[34] In this work, we synthesized a series of PS(2.2k)$_n$-*grad*-PLA(2.1k)$_m$ bottlebrush copolymers (**G1**-**G15**) with uniform side chain lengths

but varying overall compositions, with f_{PS} values ranging from 0.26 to 0.73 (Table 1). PS volume fractions of PS(2.2k)$_n$-*grad*-PLA(2.1k)$_m$ samples were readily controlled by adjusting feed ratios between *exo*-PS and *endo*-PLA via simple gravimetric measurements of the two macromonomers, which were corroborated by ^{1}H NMR analysis of the olefin signals from *exo*- and *endo*-norbornene moieties (6.25 and 6.10 ppm, respectively) in aliquots extracted from macromonomer solutions before polymerization. Complete consumption of both macromonomers were confirmed by the disappearance of the norbornene olefin signals after 16 hours. Size-exclusion chromatography (SEC) analysis evidenced the formations of bottlebrush copolymers with narrow molecular weight distributions ($Đ$ < 1.20) and minimal unreacted macromonomers (Figure 2 top, and Figure S5, Supporting Information). The near complete conversion of macromonomers minimized the impact of unreacted short macromonomer chains on polymer self-assembly.

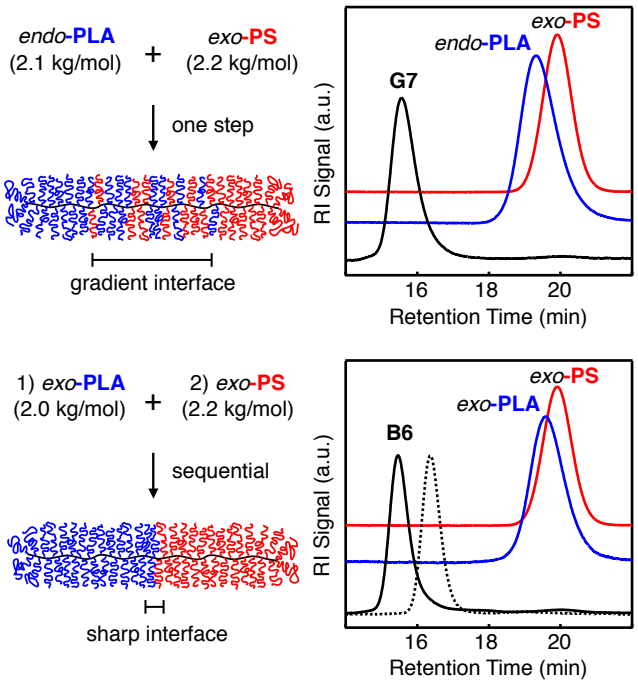

Figure 2. Synthesis and representative SEC data for gradient (**G7**) and block (**B6**) bottlebrush copolymers (dashed curve represents PLA homopolymer brush produced in the first step during block copolymer synthesis).

As a control group, a series of PS(2.2k)$_n$-*block*-PLA(2.0k)$_m$ bottlebrush block copolymers (**B1**-**B7**) were also synthesized by sequentially polymerizing *exo*-PLA (2.0 kg/mol) and *exo*-PS (2.2 kg/mol) with f_{PS} values ranging from 0.21 to 0.73 (Figure 2 bottom). Complete re-initiation and continuing growth of polymer chains was observed upon addition of the second macromonomer, as evidenced by the SEC analysis (Figure 2 and Figure S6, Supporting Information). Molecular characteristics of **G1**-**G15** and **B1**-**B7** bottlebrush copolymers are listed in Table 1. Both block and gradient bottlebrush copolymers featured PS and PLA side chains of similar lengths (~2 kg/mol) to allow us to probe specifically the effect of side chain distribution along the backbone.

Table 1. Structural parameters of PS(2.2k)$_n$-*grad*-PLA(2.1k)$_m$ (**G1**-**G15**) and PS(2.2k)$_n$-*block*-PLA(2.0k)$_m$ (**B1**-**B7**) bottlebrush copolymers with symmetric side chains.

Polymer	[PS]:[PLA][a]	$N_{backbone}$[b]	M_n (kg/mol)[c]	$Đ$[d]	f_{PS}[e]	d (nm)[f]	Morphology[g]
G1	0.27	103	213	1.15	0.26	N/A	DIS
G2	0.30	99	205	1.15	0.28	23	L+
G3	0.34	108	225	1.18	0.30	24	L
G4	0.41	167	340	1.26	0.34	33	L+
G5	0.48	144	301	1.11	0.38	28	L+
G6	0.57	125	262	1.17	0.42	28	L+
G7	0.67	127	267	1.19	0.46	30	G
G8	0.67	95	201	1.15	0.46	27	G
G9	0.79	122	257	1.17	0.50	29	C
G10	0.98	125	264	1.15	0.56	29	C
G11	1.11	122	258	1.18	0.59	28	C
G12	1.30	126	268	1.15	0.62	29	C
G13	1.56	119	254	1.13	0.67	29	C
G14	1.75	128	271	1.12	0.69	29	C
G15	2.13	106	227	1.11	0.73	N/A	DIS
B1	0.22	89	198	1.12	0.21	32	C
B2	0.32	98	217	1.11	0.28	38	L
B3	0.47	128	267	1.09	0.37	38	L
B4	0.95	136	280	1.19	0.55	52	L
B5	1.35	94	207	1.07	0.61	38	L+
B6	1.74	107	235	1.08	0.67	41	C
B7	2.00	120	252	1.08	0.73	N/A	DIS

[a]Molar ratios of macromonomers used during synthesis; [b]Total number of repeat units in the backbone $N_{backbone}$ = n + m; [c]Measured by SEC-LS; [d]Measured by SEC with linear PS calibration; [e]Volume fractions of PS determined by using the following densities: ρ_{PS} = 1.04 g/cm^3 and ρ_{PLA} =

1.25 g/cm^3; [f]Calculated as $d = 2\pi/q^*$; [f]Obtained from SAXS (DIS: disordered, L: lamellar, L+: mixed morphologies including lamellar, G: gyroid, C: cylindrical).

Self-assembly of block BCPs

We first examined the phase behavior of PS(2.2k)$_n$-*block*-PLA(2.0k)$_m$ bottlebrush copolymers to establish the morphological spectrum of copolymers with a sharp compositional transition along the backbone. Diblock bottlebrush copolymers **B1**-**B7** were comprised of side chains with equivalent lengths, and their composition was varied as a result of backbone asymmetry only. Polymer samples pressed into discs and thermally annealed at 180 °C for 16 hours were analyzed by SAXS at room temperature (Figure 3). Copolymers **B2**-**B5** showed scattering consistent with a lamellar morphology (L), where a number of higher order reflections were identified at multiples of the primary scattering peak (q^*). It must be noted that sample **B5** also showed a broad reflection centered at $\sqrt{7}q^*$, which might be indicative of the presence of some cylindrical domains in addition to lamellar domains (L+). Copolymers **B1** and **B6** showed scattering consistent with a hexagonally packed cylindrical morphology (C), as evidenced by prominent reflections at $\sqrt{3}q^*$ and $\sqrt{7}q^*$. Copolymer **B7**, with the largest PS volume fraction, did not show strong higher order reflections likely due to poor ordering, and was labeled as "disordered" (D). The morphology map constructed based on this data (Figure 3) clearly illustrated the presence of a large lamellar window spanning from $f_{PS} = 0.28$ to 0.61.This is consistent with what was observed for PS-PEO bottlebrush block copolymers.[20] The stabilization of the lamellar phase was predicted for bottlebrush block copolymers with increasing backbone stiffness.[37] Additionally, in a recent computational study of the phase separation of worm-like linear block copolymers, Chen et al. demonstrated that increasing the copolymer persistence length significantly widens the

lamellar window in the morphology diagram.[38] Within this framework, the strong propensity of bottlebrush block copolymers to form flat interfaces as compared to their linear block copolymer analogs can be attributed to their increased molecular rigidity.

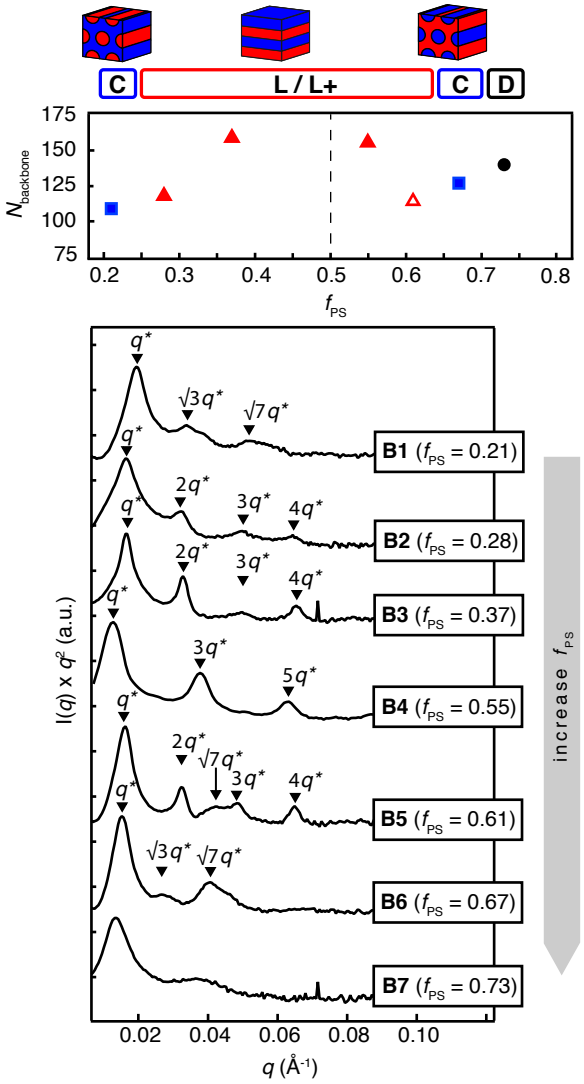

Figure 3. SAXS analysis and morphology diagram of PS(2.2k)$_n$-*block*-PLA(2.0k)$_m$ copolymers (▲ L: lamellar, △ L+: mixed morphologies including lamellar, ■ C: cylindrical, ● D: disordered).

Self-assembly of gradient BCPs with symmetric side chains

SAXS characterization of melt pressed gradient bottlebrush copolymers PS(2.2k)$_n$-*grad*-PLA(2.1k)$_m$ samples with the same side chains as their block copolymer analogs revealed a drastically different behavior (Figure 4). Copolymers **G9**-**G14** with f_{PS} ranging from 0.50 to 0.69 exhibited scattering consistent with a hexagonally packed cylindrical morphology. Depending on the composition, higher order reflections with varying intensities at $\sqrt{3}q^*$, $2q^*$, $\sqrt{7}q^*$, and $3q^*$ were observed (Figure S7 in the Supporting Information), likely due to the effect of changing form factor of PLA cylinders with varying polymer asymmetry and the coincidence of the form factor zeros with the structure factor scattering maxima[39] (within this compositional window, the domain spacing remained constant at ~29 nm, while PLA cylinder diameter ranged from 20 to 25 nm). Such a wide cylindrical morphology window is an unusual feature of the gradient bottlebrush copolymer assembly, where even the compositionally symmetric sample **G9** with symmetric side chains packs into cylindrical microstructures. At lower PS volume fractions (f_{PS} = 0.46), we observed a bicontinuous gyroid morphology for copolymers **G7** and **G8**, as evidenced by the presence of scattering maxima at q values with the following relationship: $\sqrt{6}$:$\sqrt{8}$:$\sqrt{14}$:$\sqrt{16}$:$\sqrt{20}$:$\sqrt{22}$ (Figures 4 and 5). The 2D-SAXS analysis of the smaller molecular weight gyroid-forming copolymer **G8** produced a spot pattern, instead of typically observed isotropic rings, indicating the presence of large and well-ordered grains in the sample (Figure 5). To the best of our knowledge, this is the first example of a gyroid morphology observed in a non-Janus-type bottlebrush copolymer.

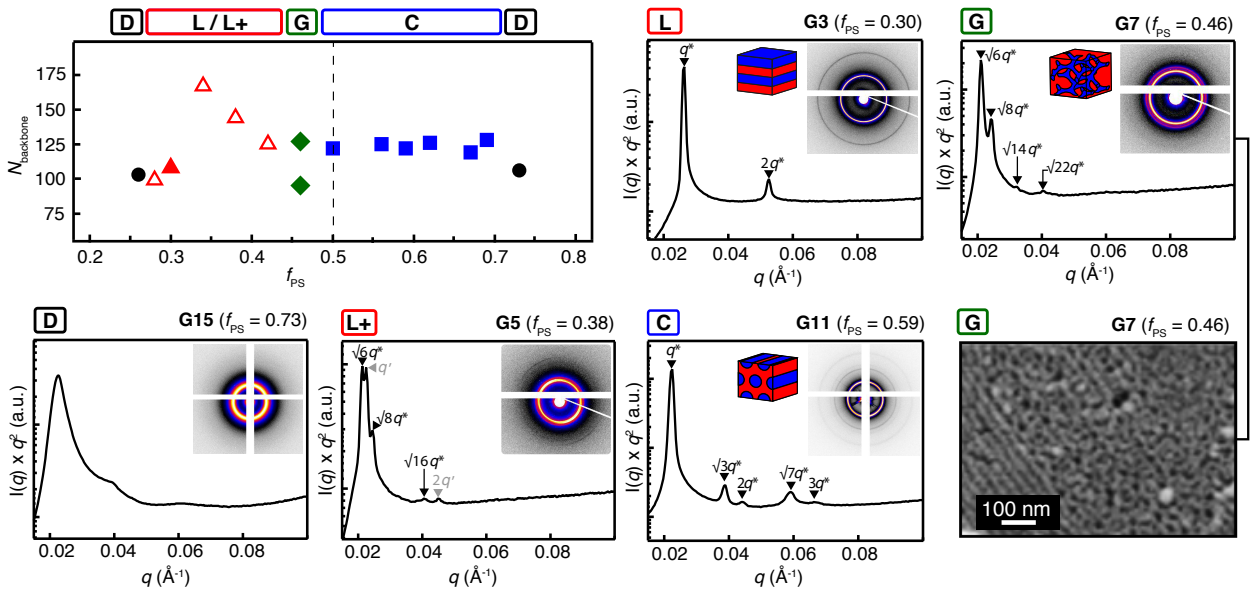

Figure 4. Morphology diagram of PS(2.2k)$_n$-*grad*-PLA(2.1k)$_m$, SAXS characterization of **G3**, **G5**, **G7**, **G11** and **G15**, and SEM image of **G7** (▲ L: lamellar, △ L+: mixed morphologies including lamellar, ■ C: cylindrical, ◆ G: gyroid, ● D: disordered).

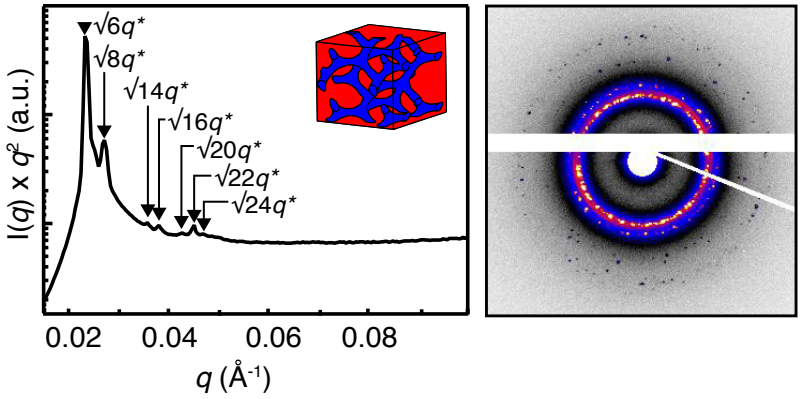

Figure 5. 2D-SAXS analysis of gyroid-forming gradient bottlebrush copolymer **G8**.

Lamellar domains were observed for copolymers **G2**-**G6**, but only highly asymmetric PLA-rich copolymer **G3** with $f_{PS} = 0.30$ exhibited scattering consistent with a well-ordered lamellar morphology, which was identified by the presence of a sharp primary scattering peak and a sharp higher order reflection at $2q^*$ (Figure 4 and Figure S8, Supporting Information). All other samples in this region (L+) exhibited either incomplete ordering with broad shoulders around the primary scattering peak, or well-identifiable mixed morphologies. For example, samples **G4** and **G6** exhibited scattering maxima at q^* and $2q^*$, which could be attributed to the presence of lamellar morphology, but they also contained large and broad shoulders at $q < q^*$. Dalsin et al. observed similar peaks in their analysis of polypropylene-polystyrene bottlebrush block copolymers, which they attributed to the kinetically trapped morphologies, such as local disorder.[40] On the other hand, copolymer **G5** at $f_{PS} = 0.38$ exhibited well-defined scattering peaks that could be attributed to the presence of both lamellar (q', $2q'$) and gyroid ($\sqrt{6}q^*$, $\sqrt{8}q^*$) domains. A quick SAXS analysis of this sample at different temperatures (Figure 6) revealed a likely order-order transition with the gyroid phase stabilized at higher temperatures. While the lab machine used for temperature-dependent SAXS studies had a lower resolution than what could be achieved at a synchrotron beamline (Figure 4), the results provided sufficient evidence for a morphological transition. At room temperature, the main peak at $q^* = 0.0222$ Å^{-1} for sample **G5** appeared broad with shoulders on both sides, and a higher order reflection at $2q^*$ was also present, consistent with mixed morphology and the presence of the lamellar phase, as described above. When heated to 130 ºC, the main scattering peak split into two maxima at scattering vector q values that were related by a ratio of $\sqrt{6}$:$\sqrt{8}$ (labelled as stars in Figure 6). Additionally, the higher order reflection at $2q^*$ disappeared. We attributed this transition to the stabilization of

the gyroid phase and disappearance of the lamellar morphology at higher temperatures. The gyroid morphology was stable up to 190 ºC. Interestingly, heating the sample from 130 ºC to 190 ºC caused the first scattering peak to move to smaller q values, from 0.0209 Å^{-1} to 0.0198 Å^{-1}, indicating an increase in domain spacing with temperature. Such a temperature dependence is opposite to what is typically observed for block copolymers, where increasing temperature leads to a decrease in the χ parameter ($\chi \sim 1/T$) and the corresponding small decrease in the domain spacing ($d \sim \chi^{1/6}$).[41] When copolymer **G5** was cooled down from 190 ºC back to room temperature, the primary peak maximum shifted back to $q^* = 0.0222$ Å^{-1}, the second scattering maxima disappeared, and the higher order reflection at $2q^*$ reappeared, suggesting a return of the lamellar phase. It is possible that depending on the cooling conditions, complete transformation to the lamellar phase is not achieved, and the sample could be trapped in a mixed phase state.

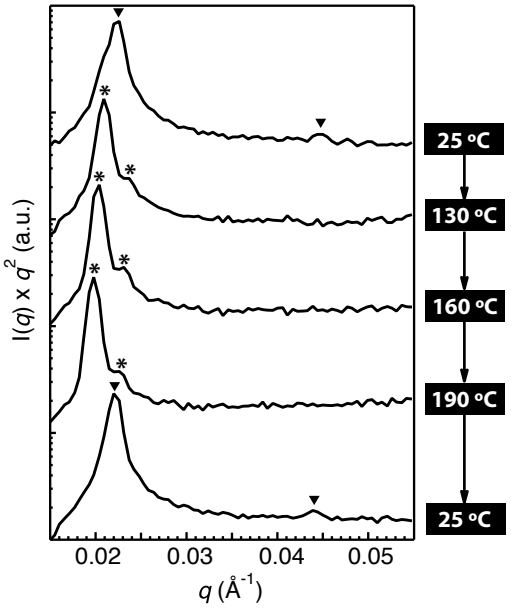

Figure 6. SAXS analysis of gradient copolymer **G5** at different temperatures. Triangles indicate signals indexing as (q, $2q$) and stars indicate signals indexing as ($\sqrt{6}q$, $\sqrt{8}q$).

The most asymmetric samples **G1** and **G15** exhibited broad primary scattering peaks and additional broad reflections (Figure 4 and Figure S8, Supporting Information), which was attributed to the formation of poorly ordered microstructures at both ends of the spectrum. No other morphologies, including the inverted cylindrical morphology at low PS volume fractions, could be identified by SAXS analysis.

Block *vs* gradient BCPs

The comparison between the melt state assemblies of block and gradient bottlebrush copolymers revealed a striking difference in the domain spacings obtained by the two copolymer systems with otherwise identical size and chemical compositions. We have previously reported that the domain spacing of symmetric gradient bottlebrush copolymers increases nearly linearly with the backbone length, but is consistently smaller than that of their block bottlebrush analogs.[34] However, that comparison was imperfect since the two systems exhibited different morphologies (lamellar for block copolymers, and cylindrical for gradient copolymers). In this work, we have prepared two sets of copolymers that can provide a more accurate assessment of the effect of gradient interface on microstructure domain spacings. For example, copolymers **G3** and **B2** have been synthesized to have similar molecular weights, side chain and backbone lengths, and PS volume fractions, with only major difference between the two being the distribution of side chains along the backbone. They both produce lamellar morphology, but the domain spacing ($d = 2\pi/q^*$) for the gradient bottlebrush copolymer **G3** is 24 nm, while for **B2** is 39 nm. Similarly, copolymers **G13** and **B6** are structurally similar and produce cylindrical morphology, but differ

significantly in the measured domain spacings (29 nm for gradient copolymer **G12**, and 41 nm for block copolymer **B6**). This represents 30-40% reduction in domain spacing by introducing a gradient interface between the two blocks. Interestingly, such a strong effect on domain spacing is not observed in linear copolymer assembly. For example, Epps et al. studied melt self-assembly of linear polystyrene-polyisoprene block copolymer with a gradient interface between the blocks where the gradient interface occupied 28% of the copolymer (tapered polymers) and observed no significant difference in lamellar domain spacings between the copolymer with the gradient interface (20.1 nm) and its analog with the sharp interface (18.4 nm).[42] These results demonstrate an important difference between bottlebrush and linear copolymer systems and indicate a strong influence of the gradient composition on the bottlebrush copolymer assembly.

The origin of this effect on domain spacing can be rationalized in terms of molecular orientation at the interface. For bottlebrush block copolymers, it has been postulated both experimentally and computationally that the bottlebrush backbone is orientated perpendicularly to the domain interface (at least within ~10 nm of the interface).[40] As a result, these copolymers produce materials with large domain spacings commensurate with the length of the backbone. For statistical and Janus-type bottlebrush copolymers, it has been observed that the domain spacing does not depend on the bottlebrush backbone length and is primarily determined by the length of the side chains, which suggests a parallel orientation of the bottlebrush backbone to the domain interface.[25,43] We reported earlier that a statistical PS-PLA bottlebrush copolymer with 2 kg/mol side chains does not produce an ordered morphology, but exhibits a broad scattering peak corresponding to a characteristic distance $d \sim 12$ nm.[34] It is reasonable to hypothesize then that gradient bottlebrush copolymers, described in this work, orient at an intermediate angle relative to the domain interface during assembly resulting in domain spacings with weaker dependence

on the bottlebrush backbone length, producing values that are smaller than their block copolymer analogs but larger than statistical copolymers with the same side chain lengths (Figure 7).

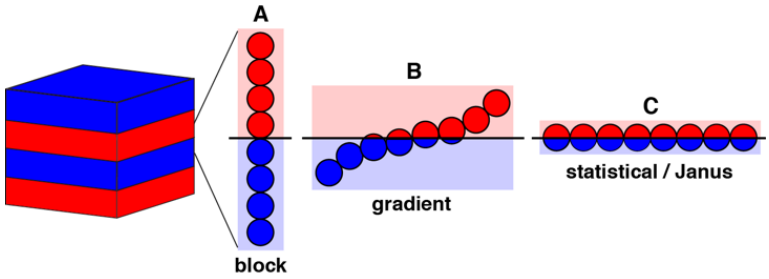

Figure 7. Coarse-grained illustration of the interfacial molecular orientation of bottlebrush copolymers with blocky (A), gradient (B), and statistical (C) distributions of side chains along the backbone.

Another important feature of the PS(2.2k)$_n$-*grad*-PLA(2.1k)$_m$ morphology diagram (Figure 4) is its highly asymmetric nature: cylindrical phase at symmetric compositions, lamellar phase at low polystyrene volume fractions, and no inverted cylindrical phase for PLA-rich (low f_{PS}) copolymers. We posit that this asymmetry could be attributed to the difference in rigidity between the PS and PLA bottlebrush components. Indeed, a number of computational studies on semiflexible-flexible block copolymers, or in the extreme case rod-coil block copolymers, predict a highly asymmetric phase diagram skewed toward higher volume fractions of the semiflexible component.[44-46] For example, lamellar phase was observed only for highly asymmetric compositions with higher volume fractions of the semiflexible component, while cylindrical phase was observed for symmetric compositions and those with higher volume

fractions of the flexible component. Additionally, no inverted cylindrical morphology was predicted at higher volume fractions of the semiflexible component. These qualitative similarities between our system and a semiflexible-flexible copolymer assembly prompted us to assess the molecular rigidity of the constituent bottlebrush blocks. We measured persistence lengths (l_p) of PS(2.2k) (M_n = 825 kg/mol, $Đ$ = 1.24) and PLA(2.0k) (M_n = 875 kg/mol, $Đ$ = 1.12) homopolymer bottlebrushes by SAXS analysis in theta solvents (acetone for PLA,[47] and cyclohexane for PS[48]) to emulate chain dimensions in the melt. Scattering from dilute solutions (2 mg/ml) was analyzed using a flexible cylinder model as implemented in SasView package.[35] The model is based on a parametrized scattering function for semiflexible chains[36] and provided l_p values of 9 nm for PLA bottlebrushes, and 2-3 nm for PS bottlebrushes (Figure S9, Supporting Information). The larger uncertainty for PS bottlebrushes l_p stems from a limited applicability of the flexible cylinder model when l_p is close to the cylinder diameter. While the obtained values were unexpectedly small, they reflected the reported chain softening by mutual interactions for bottlebrush copolymer melts.[49] Importantly, higher rigidity of the PLA bottlebrush block is consistent with the morphology diagram of the PS(2.2k)$_n$-*grad*-PLA(2.1k)$_m$ copolymers being skewed toward high PLA content, i.e. the observation of the lamellar morphology at high PLA volume fractions, and cylindrical morphology for symmetric and high PS content copolymers. Similar asymmetry, albeit to a much smaller extent, can also be observed for PS(2.2k)$_n$-*block*-PLA(2.0k)$_m$ copolymers (Figure 3). The asymmetry effect seems to be much more pronounced for gradient copolymers, for which we have no explanation, but speculate that it could be related to the molecular orientation of bottlebrush copolymers at the interface.

Self-assembly of gradient BCPs with asymmetric side chains

We have also synthesized a series of gradient bottlebrush copolymers where in addition to the compositional change along the backbone there was a gradient change in average bottlebrush diameter. This was achieved by using the same one-step copolymerization of *exo*- and *endo*-norbornene-functionalized macromonomers but with different chain lengths (Figure 8). For this series of copolymers, we used PS macromonomer with M_n = 2.2 kg/mol and a much larger PLA macromonomer with M_n = 3.7 kg/mol. Bottlebrush copolymers with varying PS volume fractions and nearly identical overall backbone lengths were prepared by adjusting the feed ratios of the macromonomers (Table 2). Even with the larger *endo*-PLA macromonomer, complete conversions were observed within 16 hours (Figure 8 and Figure S10, Supporting Information).

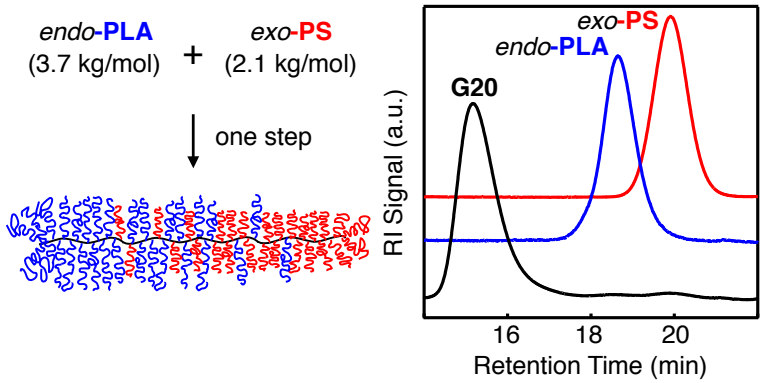

Figure 8. Synthesis and SEC analysis of gradient BCPs PS(2.2k)$_n$-*grad*-PLA(3.7k)$_m$ with asymmetric side chains.

Table 2. Structural parameters of gradient BCPs with asymmetric side chains, PS(2.2k)$_n$-*grad*-PLA(3.7k)$_m$.

Polymer	[PS]:[PLA][a]	$N_{backbone}$[b]	M_n (kg/mol)[c]	$Đ$[d]	f_{PS}[e]	d (nm)[f]	Morphology[g]
G16	0.65	76	213	1.30	0.31	28	L+
G17	0.73	79	205	1.28	0.34	26	L
G18	0.97	76	225	1.25	0.40	27	L+
G19	1.08	89	262	1.25	0.43	N/A	DIS
G20	1.54	77	267	1.21	0.52	28	C
G21	2.17	79	201	1.20	0.60	27	C
G22	3.03	84	258	1.14	0.68	26	C

[a]Molar ratios of macromonomers used during synthesis; [b]Total number of repeat units in the backbone $N_{backbone}$ = n + m; [c]Measured by SEC-LS; [d]Measured by SEC with linear PS calibration; [e]Volume fractions of PS determined by using the following densities: ρ_{PS} = 1.04 g/cm^3 and ρ_{PLA} = 1.25 g/cm^3; [f]Calculated as $d = 2\pi/q^*$; [g]Obtained from SAXS (DIS: disordered, L: lamellar, L+: mixed morphologies including lamellar, C: cylindrical).

Self-assembly of PS(2.2k)$_n$-*grad*-PLA(3.7k)$_m$ gradient bottlebrush copolymers was studied by SAXS analysis of the melt pressed samples (Figure 9). Samples **G20**-**G22** with f_{PS} = 0.68 - 0.52 exhibited scattering consistent with a hexagonally packed cylindrical morphology, as evidenced by the presence of either $\sqrt{3}q^*$ or $\sqrt{7}q^*$ peaks, or both. Here again, the absence of certain higher order reflections is likely due to their coincidence with the cylinder form factor zeros. Copolymers **G16**-**G18** formed lamellar microstructures, indicated by the presence of sharp q^* and $2q^*$ peaks. However, primary scattering peaks in samples **G16** and **G18** were accompanied by broad shoulders on either side, which were indicative or poor or incomplete ordering. Copolymer **G19** with f_{PS} = 0.43 located between the cylindrical and lamellar regions only exhibited broad scattering peaks and was labelled as "disordered" in the morphology diagram.

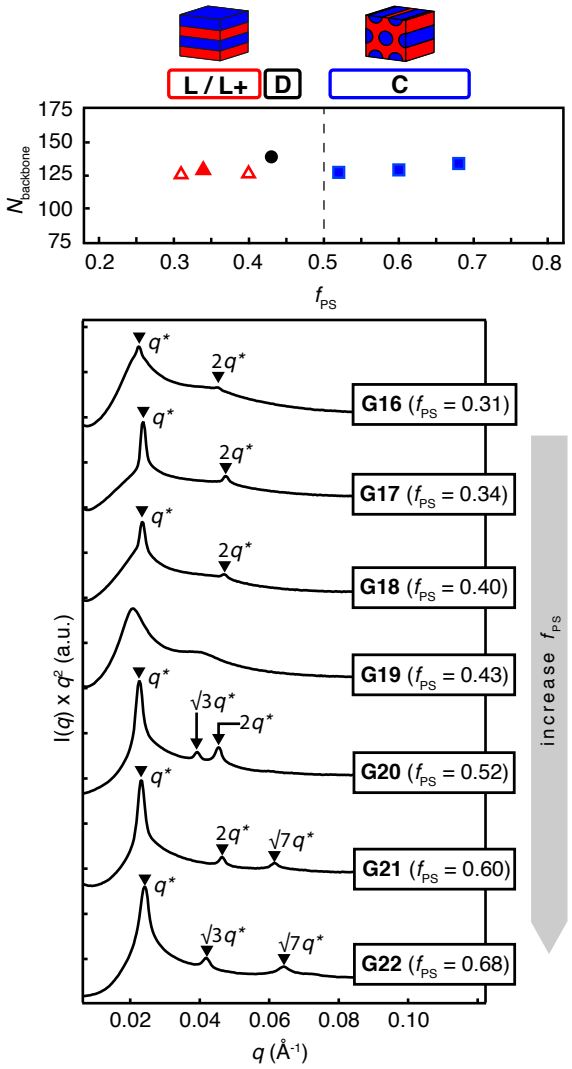

Figure 9. SAXS analysis and morphology diagram of side-chain-asymmetric gradient BCPs PS(2.2k)$_n$-*grad*-PLA(3.7k)$_m$ (▲ L: lamellar, △ L+: mixed morphologies including lamellar, ■ C: cylindrical, ● D: disordered).

We initially expected that increasing the cross-sectional diameter of the PLA brush will curve the interface toward the PS domain, which will result in a more symmetric morphology diagram. For example, it was previously reported that bottlebrush block copolymers with asymmetric side

chains will form cylindrical microstructures where the cylinder domains are formed by the bottlebrush block with smaller side chains.[23,50] However, the morphology diagram for side-chain-asymmetric gradient copolymers PS(2.2k)$_n$-*grad*-PLA(3.7k)$_m$ constructed using the SAXS data (Figure 9) bears key similarities to that of the side-chain-symmetric samples PS(2.2k)$_n$-*grad*-PLA(2.1k)$_m$ discussed earlier (Figure 4): (1) cylindrical morphology is observed in a wide compositional window (f_{PS} = 0.52 – 0.68), including for nearly compositionally symmetric copolymers, and (2) lamellar phase is observed only for high PLA-content copolymers (f_{PS} = 0.31 and 0.40). This implies that these gradient copolymers tend to pack into cylindrical microstructures with PLA cylinders even though PLA brush component has a larger cross-sectional diameter. It is possible that increasing the side chain length of the PLA brushes resulted in increased stiffness, as has been reported for other bottlebrush copolymer systems,[51-53] which produced the opposite effect on the morphology diagram. While this phenomenon is under further investigation, it is clear that gradient bottlebrush copolymers provide easy access to a well-ordered cylindrical morphology, which is of interest in a variety of applications, such as surface patterning and membrane fabrication.

Conclusion

The one-step ROMP synthesis of compositionally gradient PS-PLA bottlebrush copolymers from *exo*- and *endo*-norbornene-functionalized macromonomers enabled rapid access to a library of copolymers with varying volume fractions. Melt self-assembly of these gradient bottlebrush copolymers across a wide range of PS volume fractions produced materials with a variety of morphologies, as determined by SAXS. In a striking contrast to their bottlebrush block

copolymer analogs, the morphological map of gradient BCPs exhibited a wide cylindrical morphology window, including for symmetric compositions, while well-ordered lamella microstructures were only observed for high PLA-content copolymers. Additionally, a rare bicontinuous gyroid morphology was observed for gradient BCPs with $f_{PS} = 0.46$.

Domain spacings of gradient bottlebrush copolymers were significantly smaller (by 30-40%) than those of their block BCP analogs with the same size, composition and morphology. The difference in domain spacings between the block and gradient bottlebrush copolymers, which is a unique behavior not observed in linear systems, was attributed to the interfacial localization of the gradient portion of the copolymer and a non-perpendicular orientation of the gradient bottlebrush backbone relative to the domain interface. The morphology diagram of the gradient bottlebrush copolymers was highly asymmetric with a wide cylindrical morphology window for PS-rich copolymers and a complete absence of the inverted cylindrical morphology at high PLA volume fractions, which was attributed to the difference in molecular rigidity between PLA and PS brush components, as determined by SAXS.

Gradient BCPs with asymmetric side chains were also prepared by using macromonomers with different molecular weights. These “cone” shaped molecules with a gradient change in average cross-sectional diameter along the backbone packed into well-ordered cylindrical and lamellar microstructures. It appears that for this specific system, volume fraction of the components, and not the side chain asymmetry, was the dominant factor governing their morphological behavior.

The results described in this paper indicate that the gradient interface in bottlebrush copolymers can be used as an effective handle in controlling molecular packing. The combination of “user-

friendly" one-step synthesis and a rich morphological behavior of gradient bottlebrush copolymers presents a versatile platform for nanostructured materials development.

ASSOCIATED CONTENT

Supporting Information

Supporting Information is available free of charge on the ACS Publication website.

NMR characterization of macromonomers, SEC and SAXS characterization of bottlebrush copolymers (PDF).

AUTHOR INFORMATION

Corresponding Author

*Email: jrzayev@buffalo.edu

Notes

The authors declare no competing financial interest.

ACKNOWLEDGMENT

Financial support was provided by the National Science Foundation (DMR-1709371). This research used resources of the Center for Functional Nanomaterials and CMS beamline of the National Synchrotron Light Source II, a U.S. Department of Energy (DOE) Office of Science User Facilities operated for the DOE Office of Science by Brookhaven National Laboratory under Contract No. DE-SC0012704. This work benefited from the use of the SasView application, originally developed under NSF Award DMR-0520547. SasView also contains code

developed with funding from the EU Horizon 2020 programme under the SINE2020 project Grant No 654000.

REFERENCES

(1) Jackson, E. A.; Hillmyer, M. A. Nanoporous Membranes Derived from Block Copolymers: From Drug Delivery to Water Filtration *ACS Nano* **2010,** *4*, 3548-3553.

(2) Stefik, M.; Guldin, S.; Vignolini, S.; Wiesner, U.; Steiner, U. Block Copolymer Self-Assembly for Nanophotonics *Chemical Society Reviews* **2015,** *44*, 5076-5091.

(3) Abetz, V.; Simon, P. F. W., Phase Behaviour and Morphologies of Block Copolymers. In *Block Copolymers I*, Abetz, V., Ed. Springer Berlin Heidelberg: Berlin, Heidelberg, 2005; pp 125-212.

(4) Yoon, J.; Lee, W.; Thomas, E. L. Self-Assembly of Block Copolymers for Photonic-Bandgap Materials *MRS Bulletin* **2005,** *30*, 721-726.

(5) Orilall, M. C.; Wiesner, U. Block Copolymer Based Composition and Morphology Control in Nanostructured Hybrid Materials for Energy Conversion and Storage: Solar Cells, Batteries, and Fuel Cells *Chemical Society Reviews* **2011,** *40*, 520-535.

(6) Bates, C. M.; Bates, F. S. 50th Anniversary Perspective: Block Polymers—Pure Potential *Macromolecules* **2017,** *50*, 3-22.

(7) Matsen, M. W.; Bates, F. S. Unifying Weak- and Strong-Segregation Block Copolymer Theories *Macromolecules* **1996,** *29*, 1091-1098.

(8) Bates, F. S.; Fredrickson, G. H. Block Copolymer Thermodynamics: Theory and Experiment *Annual Review of Physical Chemistry* **1990,** *41*, 525-557.

(9) Bates, F. S. Polymer-Polymer Phase-Behavior *Science* **1991,** *251*, 898-905.

(10) Bates, F. S.; Fredrickson, G. H. Block Copolymer Thermodynamics - Theory and Experiment *Annu. Rev. Phys. Chem.* **1990,** *41*, 525-557.

(11) Sheiko, S. S.; Sumerlin, B. S.; Matyjaszewski, K. Cylindrical Molecular Brushes: Synthesis, Characterization, and Properties *Progress in Polymer Science* **2008,** *33*, 759-785.

(12) Verduzco, R.; Li, X.; Pesek, S. L.; Stein, G. E. Structure, Function, Self-Assembly, and Applications of Bottlebrush Copolymers *Chemical Society Reviews* **2015,** *44*, 2405-2420.

(13) Rzayev, J. Molecular Bottlebrushes: New Opportunities in Nanomaterials Fabrication *ACS Macro Letters* **2012,** *1*, 1146-1149.

(14) Gu, W.; Huh, J.; Hong, S. W.; Sveinbjornsson, B. R.; Park, C.; Grubbs, R. H.; Russell, T. P. Self-Assembly of Symmetric Brush Diblock Copolymers *ACS Nano* **2013,** *7*, 2551-2558.

(15) Rzayev, J. Synthesis of Polystyrene - Polylactide Bottlebrush Block Copolymers and Their Melt Self-Assembly into Large Domain Nanostructures *Macromolecules* **2009,** *42*, 2135-2141.

(16) Sveinbjoernsson, B. R.; Weitekamp, R. A.; Miyake, G. M.; Xia, Y.; Atwater, H. A.; Grubbs, R. H. Rapid Self-Assembly of Brush Block Copolymers to Photonic Crystals *Proc. Natl. Acad. Sci. U. S. A.* **2012,** *109*, 14332-14336.

(17) Macfarlane, R. J.; Kim, B.; Lee, B.; Weitekamp, R. A.; Bates, C. M.; Lee, S. F.; Chang, A. B.; Delaney, K. T.; Fredrickson, G. H.; Atwater, H. A.; Grubbs, R. H. Improving Brush Polymer

Infrared One-Dimensional Photonic Crystals Via Linear Polymer Additives *J. Am. Chem. Soc.* **2014,** *136*, 17374-17377.

(18) Runge, M. B.; Bowden, N. B. Synthesis of High Molecular Weight Comb Block Copolymers and Their Assembly into Ordered Morphologies in the Solid State *J. Am. Chem. Soc.* **2007,** *129*, 10551-10560.

(19) Rzayev, J. Synthesis of Polystyrene–Polylactide Bottlebrush Block Copolymers and Their Melt Self-Assembly into Large Domain Nanostructures *Macromolecules* **2009,** *42*, 2135-2141.

(20) Gai, Y.; Song, D.-P.; Yavitt, B. M.; Watkins, J. J. Polystyrene-Block-Poly(Ethylene Oxide) Bottlebrush Block Copolymer Morphology Transitions: Influence of Side Chain Length and Volume Fraction *Macromolecules* **2017,** *50*, 1503-1511.

(21) Xia, Y.; Olsen, B. D.; Kornfield, J. A.; Grubbs, R. H. Efficient Synthesis of Narrowly Dispersed Brush Copolymers and Study of Their Assemblies: The Importance of Side Chain Arrangement *J. Am. Chem. Soc* **2009,** *131*, 18525-18532.

(22) Bates, C. M.; Chang, A. B.; Momčilović, N.; Jones, S. C.; Grubbs, R. H. Aba Triblock Brush Polymers: Synthesis, Self-Assembly, Conductivity, and Rheological Properties *Macromolecules* **2015,** *48*, 4967-4973.

(23) Bolton, J.; Bailey, T. S.; Rzayev, J. Large Pore Size Nanoporous Materials from the Self-Assembly of Asymmetric Bottlebrush Block Copolymers *Nano Lett.* **2011,** *11*, 998-1001.

(24) Choo, Y.; Mahajan, L. H.; Gopinadhan, M.; Ndaya, D.; Deshmukh, P.; Kasi, R. M.; Osuji, C. O. Phase Behavior of Polylactide-Based Liquid Crystalline Brushlike Block Copolymers *Macromolecules* **2015,** *48*, 8315-8322.

(25) Kawamoto, K.; Zhong, M.; Gadelrab, K. R.; Cheng, L.-C.; Ross, C. A.; Alexander-Katz, A.; Johnson, J. A. Graft-through Synthesis and Assembly of Janus Bottlebrush Polymers from a-Branch-B Diblock Macromonomers *J. Am. Chem. Soc.* **2016,** *138*, 11501-11504.

(26) Nguyen, H. V. T.; Gallagher, N. M.; Vohidov, F.; Jiang, Y.; Kawamoto, K.; Zhang, H.; Park, J. V.; Huang, Z.; Ottaviani, M. F.; Rajca, A.; Johnson, J. A. Scalable Synthesis of Multivalent Macromonomers for Romp *ACS Macro Letters* **2018,** *7*, 472-476.

(27) Chang, A. B.; Lin, T.-P.; Thompson, N. B.; Luo, S.-X.; Liberman-Martin, A. L.; Chen, H.-Y.; Lee, B.; Grubbs, R. H. Design, Synthesis, and Self-Assembly of Polymers with Tailored Graft Distributions *J. Am. Chem. Soc.* **2017,** *139*, 17683-17693.

(28) Lee, H. I.; Matyjaszewski, K.; Yu, S.; Sheiko, S. S. Molecular Brushes with Spontaneous Gradient by Atom Transfer Radical Polymerization *Macromolecules* **2005,** *38*, 8264-8271.

(29) Borner, H. G.; Duran, D.; Matyjaszewski, K.; da Silva, M.; Sheiko, S. S. Synthesis of Molecular Brushes with Gradient in Grafting Density by Atom Transfer Polymerization *Macromolecules* **2002,** *35*, 3387-3394.

(30) Radzinski, S. C.; Foster, J. C.; Scannelli, S. J.; Weaver, J. R.; Arrington, K. J.; Matson, J. B. Tapered Bottlebrush Polymers: Cone-Shaped Nanostructures by Sequential Addition of Macromonomers *ACS Macro Lett.* **2017,** *6*, 1175-1179.

(31) Walsh, D. J.; Guironnet, D. Macromolecules with Programmable Shape, Size, and Chemistry *Proc. Natl. Acad. Sci. U. S. A.* **2019,** *116*, 1538-1542.

(32) Kim, K. O.; Choi, T. L. Synthesis of Dendronized Polymers Via Macromonomer Approach by Living Romp and Their Characterization: From Rod-Like Homopolymers to Block and Gradient Copolymers *Macromolecules* **2013,** *46*, 5905-5914.

(33) Jiang, L.; Nykypanchuk, D.; Ribbe, A. E.; Rzayev, J. One-Shot Synthesis and Melt Self-Assembly of Bottlebrush Copolymers with a Gradient Compositional Profile *ACS Macro Letters* **2018**, 619-623.

(34) Jiang, L.; Nykypanchuk, D.; Ribbe, A. E.; Rzayev, J. One-Shot Synthesis and Melt Self-Assembly of Bottlebrush Copolymers with a Gradient Compositional Profile *ACS Macro Lett*. **2018,** *7*, 619-623.

(35) Doucet, M., et al. *Sasview*, version 4.1.2; Zenodo, August 2017. http://doi.org/10.5281/zenodo.825675

(36) Pedersen, J. S.; Schurtenberger, P. Scattering Functions of Semiflexible Polymers with and without Excluded Volume Effects *Macromolecules* **1996,** *29*, 7602-7612.

(37) Chremos, A.; Theodorakis, P. E. Impact of Intrinsic Backbone Chain Stiffness on the Morphologies of Bottle-Brush Diblock Copolymers *Polymer* **2016,** *97*, 191-195.

(38) Jiang, Y.; Chen, J. Z. Influence of Chain Rigidity on the Phase Behavior of Wormlike Diblock Copolymers *Phys Rev Lett* **2013,** *110*, 138305.

(39) Honeker, C. C.; Thomas, E. L.; Albalak, R. J.; Damian A. Hajduk; Gruner, S. M.; Capel, M. C. Perpendicular Deformation of a near-Single-Crystal Triblock Copolymer with a Cylindrical Morphology. 1. Synchrotron Saxs *Macromolecules* **2000,** *33*, 9395-9406.

(40) Dalsin, S. J.; Rions-Maehren, T. G.; Beam, M. D.; Bates, F. S.; Hillmyer, M. A.; Matsen, M. W. Bottlebrush Block Polymers: Quantitative Theory and Experiments *ACS Nano* **2015,** *9*, 12233-12245.

(41) Zalusky, A. S.; Olayo-Valles, R.; Wolf, J. H.; Hillmyer, M. A. Ordered Nanoporous Polymers from Polystyrene-Polylactide Block Copolymers *J. Am. Chem. Soc.* **2002,** *124*, 12761-12773.

(42) Luo, M.; Brown, J. R.; Remy, R. A.; Scott, D. M.; Mackay, M. E.; Hall, L. M.; Epps, T. H. Determination of Interfacial Mixing in Tapered Block Polymer Thin Films: Experimental and Theoretical Investigations *Macromolecules* **2016,** *49*, 5213-5222.

(43) Xia, Y.; Olsen, B. D.; Kornfield, J. A.; Grubbs, R. H. Efficient Synthesis of Narrowly Dispersed Brush Copolymers and Study of Their Assemblies: The Importance of Side-Chain Arrangement *J. Am. Chem. Soc.* **2009,** *131*, 18525-18532.

(44) Li, W.; Gersappe, D. Self-Assembly of Rod-Coil Diblock Copolymers *Macromolecules* **2001,** *34*, 6783-6789.

(45) Gao, J.; Tang, P.; Yang, Y. Non-Lamellae Structures of Coil–Semiflexible Diblock Copolymers *Soft Matter* **2013,** *9*, 69-81.

(46) Kumar, N. A.; Ganesan, V. Communication: Self-Assembly of Semiflexible-Flexible Block Copolymers *The Journal of Chemical Physics* **2012,** *136*.

(47) Legrand, P.; Lesieur, S.; Bochot, A.; Gref, R.; Raatjes, W.; Barratt, G.; Vauthier, C. Influence of Polymer Behaviour in Organic Solution on the Production of Polylactide Nanoparticles by Nanoprecipitation *Int J Pharm* **2007,** *344*, 33-43.

(48) Wagner, H. L. The Mark–Houwink–Sakurada Equation for the Viscosity of Atactic Polystyrene *J. Phys. Chem. Ref. Data* **1985,** *14*, 1101.

(49) Bolisetty, S.; Airaud, C.; Xu, Y.; Muller, A. H. E.; Harnau, L.; Rosenfeldt, S.; Lindner, P.; Ballauff, M. Softening of the Stiffness of Bottle-Brush Polymers by Mutual Interaction *Phys. Rev. E* **2007,** *75*, 4.

(50) Bolton, J.; Rzayev, J. Tandem RAFT-ATRP Synthesis of Polystyrene–Poly(Methyl Methacrylate) Bottlebrush Block Copolymers and Their Self-Assembly into Cylindrical Nanostructures *ACS Macro Lett.* **2012,** *1*, 15-18.

(51) Sugiyama, M.; Nakamura, Y.; Norisuye, T. Dilute-Solution Properties of Polystyrene Polymacromonomer Having Side Chains of over 100 Monomeric Units *Polym. J.* **2007,** *40*, 109-115.

(52) Rathgeber, S.; Pakula, T.; Wilk, A.; Matyjaszewski, K.; Lee, H. I.; Beers, K. L. Bottle-Brush Macromolecules in Solution: Comparison between Results Obtained from Scattering Experiments and Computer Simulations *Polymer* **2006,** *47*, 7318-7327.

(53) Zhang, B.; Grohn, F.; Pedersen, J. S.; Fischer, K.; Schmidt, M. Conformation of Cylindrical Brushes in Solution: Effect of Side Chain Length *Macromolecules* **2006,** *39*, 8440-8450.

Table of Contents Graphic